

Model Predictive Control-Based Depth Control in Gliding Motion of a Gliding Robotic Dolphin

Jian Wang^{ID}, Zhengxing Wu^{ID}, Min Tan, and Junzhi Yu^{ID}, *Senior Member, IEEE*

Abstract—This article proposes a model predictive control (MPC)-based depth control system for the gliding motion of a gliding robotic dolphin. An injector-based buoyancy-driven mechanism is employed to achieve more precise control of net buoyancy. In the system, a novel framework of depth control is proposed on the basis of a simplified model, including a depth controller with improved MPC, a heading controller with velocity-based proportional-integral-derivative, and a sliding mode observer. Extensive simulation and experimental results demonstrate the effectiveness of the proposed control methods. In particular, a variety of slider-based experiments are also conducted to explore the performance of a movable slider in the depth control so as to better govern the gliding angle. The results obtained reveal that it is feasible to realize regular gliding angles via regulating the slider, which offers promising prospects for bio-inspired gliding robots playing a key role in ocean exploration.

Index Terms—Depth control, gliding motion, model predictive control (MPC), underwater robotics.

I. INTRODUCTION

BIO-INSPIRED aquatic robots have attracted more interests of scientists in recent years, and played more important roles in applications of underwater exploration, observation, and operation [1]–[3]. Due to the low noise and high maneuverability, various biomimetic prototypes have been developed to meet practical requirements. Therein, via imitating the shape of cetaceans, robotic dolphins can perform many excellent motions, such as the

360° frontflip-backflip motion [4] and astonishing leaping action [5]. Furthermore, various motion controls have also been conducted on robotic dolphins. Yu *et al.* [6] offered motion control strategies for a robotic dolphin to achieve repetitive leaping. Wu *et al.* [7] developed a robotic dolphin to apply for water quality monitoring. In recent years, taking the energy consumption into consideration, some researchers introduced buoyancy-driven mechanisms into underwater bionic robots, such as gliding robotic dolphins [8], [9] and gliding robotic fish [10]. The combinations endowed the robots with both low energy consumption and high maneuverability, which merged the advantages of robotic dolphins and underwater gliders [11]. Based on these prototypes, some motion control problems were addressed, e.g., the heading and pitch controls for a gliding robotic dolphin [12], [13], and even some applications were tried, e.g., an autonomous sampling of water columns [14].

Depth control is a very important research topic for aquatic robots. For example, when autonomous underwater vehicles (AUVs) need to arrive the area with a specified depth for more complex ocean tasks, it is crucial to achieve steady depth control. Besides, the depth control is also an important part of navigation and path following. There exists many depth control researches for underwater robots. For the traditional AUVs, the propellers equipped in vertical plane are usually used to generate the forces to diving or surfacing, which yet may cause environment damage due to the noise. Li and Lee [15] presented an adaptive nonlinear controller by removing the assumption of a small pitch angle, and realized the depth control for an AUV. Silvestre and Pascoal [16] designed a nonlinear gain-scheduling controller, and applied the methodology to achieve depth control. Wu *et al.* [17] employed the reinforcement learning for the successful depth control. Furthermore, for traditional underwater gliders, the depth control could be realized via adjusting the buoyancy-driven mechanism [18], [19]. Nevertheless, the depth control for underwater gliders were studied by simulations more than experiments. Regarding bio-inspired aquatic robots, the pitch moments were usually controlled to achieve further depth control via movable surfaces or centroid adjustment mechanism. By regulating the movable pectoral surfaces, Yu *et al.* realized the depth control with the sliding mode fuzzy method on the prototypes of a robotic fish [20] and a robotic dolphin [21], in which the latter achieved a smaller steady error, less than 0.5 cm. Besides, Shen *et al.* [22] employed a movable slider to adjust the centroid, further achieved depth control with the 5-cm error. Moreover, Makrodimitris *et al.* [23] conducted depth

Manuscript received July 23, 2019; accepted November 18, 2019. This work was supported in part by the National Natural Science Foundation of China under Grant 61421004, Grant 61836015, Grant 61633020, Grant 61633017, and Grant 61725305, and in part by the Key Project of Frontier Science Research of Chinese Academy of Sciences under Grant QYZDJ-SSW-JSC004. This article was recommended by Associate Editor T. Li. (*Corresponding author: Junzhi Yu.*)

J. Wang, Z. Wu, and M. Tan are with the State Key Laboratory of Management and Control for Complex Systems, Institute of Automation, Chinese Academy of Sciences, Beijing 100190, China, and also with the School of Artificial Intelligence, University of Chinese Academy of Sciences, Beijing 100049, China (e-mail: wangjian2016@ia.ac.cn; zhengxing.wu@ia.ac.cn; min.tan@ia.ac.cn).

J. Yu is with the State Key Laboratory of Management and Control for Complex Systems, Institute of Automation, Chinese Academy of Sciences, Beijing 100190, China, and also with the State Key Laboratory for Turbulence and Complex System, Department of Mechanics and Engineering Science, Beijing Innovation Center for Engineering Science and Advanced Technology, College of Engineering, Peking University, Beijing 100871, China (e-mail: junzhi.yu@ia.ac.cn).

Color versions of one or more of the figures in this article are available online at <http://ieeexplore.ieee.org>.

Digital Object Identifier 10.1109/TSMC.2019.2956531

control with a pump mechanism equipped in a small robotic fish, and realized a 2-cm steady error.

From the perspective of control methods, there are many model-based control methods which have been successfully applied for AUVs, such as sliding mode control (SMC), backstepping control, and model predictive control (MPC). In recent years, MPC has been widely used in the mobile robots due to its good performances and less model dependence [24]–[26]. Generally speaking, MPC is much suitable for the underwater robot control since it can contribute to reduce the impact of the large delay. However, there were relatively fewer applications of MPC on underwater robots due to relatively complex implementation [27]–[30], and most of them were just designed in simulations. Therefore, more depth control researches of biomimetic aquatic robots with gliding motion, such as gliding robotic dolphins and gliding robotic fish, are necessary. Whereas, it is quite challenged for depth control only by buoyancy-driven mechanism due to large delay and insufficient control ability. More importantly, on the one hand, the tasks which require to arrive a target depth can be accomplished by the combination of gliding and dolphin-like motions. On the other hand, the successful depth control only by buoyancy-driven mechanism can provide the basis for the gliding robotic dolphin to achieve the hovering, which is a significant technology for underwater operation.

This article mainly focuses on the problem of depth control for a gliding robotic dolphin regulated by an injector-based buoyancy-driven mechanism in gliding motion, which has not been addressed in previous literature, to the best of our knowledge. The main contributions of this article are twofold. On the one hand, a novel depth control strategy consisting of an MPC depth controller, a velocity-PID heading controller, and a sliding mode observer (SMO) is proposed for gliding motion. Before designing these controllers, we first construct the dynamic model of a gliding robotic dolphin for simulation analysis, and further reasonably simplify it for control laws derivation. Then, with an improved reference tracking, the MPC controller is constructed for depth control, and the SMO is designed to estimate the gliding velocity. Meanwhile, considering the simplified model neglects the yaw motion, a velocity-PID heading controller is also built to keep yaw orientation in the gliding process. On the other hand, we further investigate the effect of a movable slider on the gliding angle in-depth control, which contributes to make sure the horizontal gliding distance during depth control process. Finally, various simulations and experiments are conducted to validate the effectiveness of the proposed control method. These results and analysis offer a valuable sight to the practical application of the gliding robotic dolphin.

The remainder of this article is organized as follows. Section II provides the configuration of a gliding robotic dolphin. The derivation of gliding motion for a gliding robotic dolphin is detailed in Section III. Section IV illustrates the depth control system, including an SMO, a velocity-PID heading controller, and an MPC depth controller. In Section V, both simulation and experimental results are discussed. Finally, Section VI summarizes the conclusions and future work.

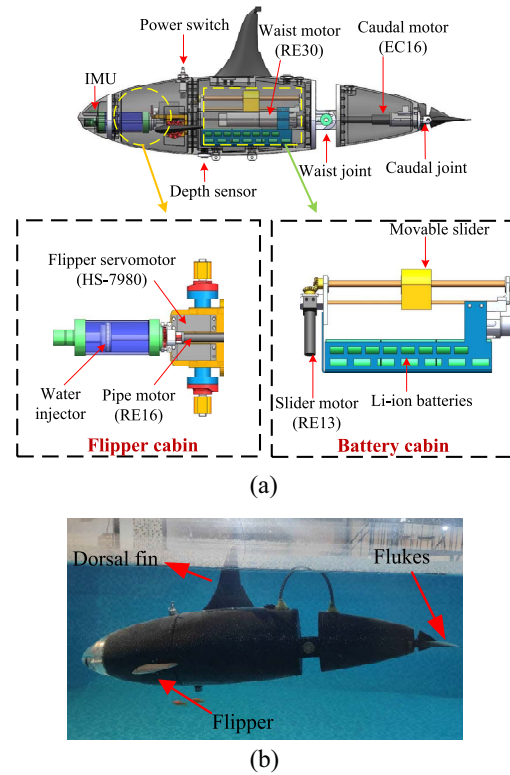


Fig. 1. Overview of the gliding robotic dolphin. (a) Conceptual design. (b) Robotic prototype.

II. OVERVIEW OF THE GLIDING ROBOTIC DOLPHIN

As illustrated in Fig. 1, the gliding robotic dolphin adopts a well-streamlined body shape via imitating a killer whale. The mechanical and electrical configurations are tabulated in Table I. As a typical combination of underwater gliders and robotic dolphins, the gliding robotic dolphin has two main parts: 1) a dolphin-like part with a dorsoventral propulsive system and 2) a gliding part with a buoyancy-centroid adjusting system.

- 1) *Dolphin-Like Part*: This part is mainly composed of two flippers and a tail cabin. Two flippers can be used to perform the deflecting motion and median and/or paired fin (MPF) motion. The robot can use this motion to achieve not only the forward/backward movements but also little-radius turn via flapping the two flippers in specific ways. Besides, the body and/or caudal fin (BCF) motion can be implemented through flapping the waist and caudal joints. The corresponding motor selections of the dolphin-like part are shown in Fig. 1(a).
- 2) *Gliding Part*: The gliding part consists of an injector-based buoyancy-driven mechanism and a slider-based pitching mechanism. The detail mechanical structure is figured in Fig. 1(a). In order to fulfill the suction and drainage, a dc brush motor (RE16) is used to drive the gear for further moving the piston. Besides, a rotating plug is employed to guarantee waterproof. Regarding the moving slider, its basic principle is almost the same as the injector's, and the difference lies in the lower power motor (RE13). Hence, the injector and slider can

TABLE I
TECHNICAL PARAMETERS OF THE GLIDING ROBOTIC DOLPHIN

Items	Characteristics
Size ($L \times W \times H$)	$\sim 0.83 \times 0.38 \times 0.33$ m ³
Total mass	~ 8.86 kg
Power supply	Li-ion Battery (DC 24.6 V, 3200 mAh)
Number of the body joints	4
Drive mode	DC motor, EC motor, servo motor
Onboard sensors	IMU (JY901), depth sensor (MS5837)
Controller	STM32F407 (168 MHz, 1 M Flash)

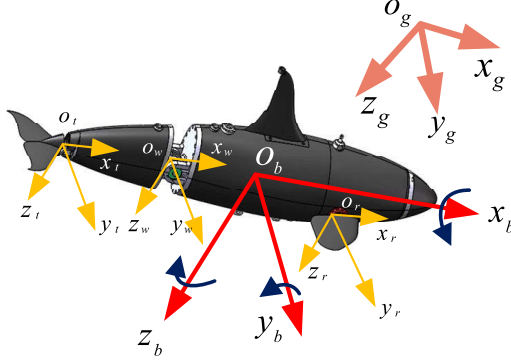


Fig. 2. Coordinate systems, including inertial, body, and fin frames.

be controlled via position mode of motors, which can realize the relatively precise buoyancy control via calculating the volume change. In detail, the total volume of the injector is approximately 0.128 L, and can yield the maximum net water mass up to 0.064 kg (here, the water density is 1000 kg/m³), which is about 0.72% of the whole displacement. Besides, the mass of slider is approximately 350 g, which can provide enough pitch moment to adjust body attitude.

III. DYNAMIC MODELING FOR GLIDING ROBOTIC DOLPHIN

First, the involved coordinate frames are illustrated in Fig. 2. $C_g = o_g x_g y_g z_g$ and $C_b = o_b x_b y_b z_b$ represent the inertia and body frames, respectively. Afterward, with the consideration of the rotatable fins surfaces, we attach $C_i = o_i x_i y_i z_i$ to each rotatable surface frame, and $i = w, t, l, r$ denote the waist, flukes, left flipper, and right flipper, respectively.

Let $U_b = (U_{bx}, U_{by}, U_{bz})^T$ and $\Omega_b = (\Omega_{bx}, \Omega_{by}, \Omega_{bz})^T$ denote the body translational velocity and angular velocity of the gliding robotic dolphin with respect to (w.r.t.) the body frame, respectively. ψ and θ illustrate the yaw and pitch angle, respectively. Furthermore, $V_b = (U_b^T, \Omega_b^T)^T$ indicate the full velocity vector. The kinematics of the robot are formalized by

$$\begin{aligned} {}^g \dot{P}_b &= {}^g U_b = {}^g R_b U_b \\ {}^g \dot{R}_b &= {}^g R_b \hat{\Omega}_b \end{aligned} \quad (1)$$

where ${}^g P_b$ and ${}^g R_b$ illustrate the position vector and rotation matrix of C_b w.r.t. C_g , respectively.

With regard to gliding motion, the equations are derived here by computing momenta from the total vehicle-fluid system energy. Let p and π denote the total translational and total angular momentum of system, respectively, which

are all expressed w.r.t. inertial frame. Let P and Π represent the momentum expressed w.r.t. body frame. Therefore, the conversion relationship between them is as follows [31]:

$$\begin{aligned} p &= RP \\ \pi &= R\Pi + l \times p \end{aligned} \quad (2)$$

where l is the vector from the origin of inertial frame to the origin of body frame. Furthermore, denote T as the system total kinetic energy, and T_i ($i = b, f, m, s$) represents the body, additional, movable mass, and injector kinetic energy, respectively. The total kinetic energy T is computed as follows:

$$\begin{aligned} T &= T_b + T_f + T_m + T_s \\ &= \frac{1}{2} (U_b^T \Omega_b^T) \tilde{M} \begin{pmatrix} U_b \\ \Omega_b \end{pmatrix} \\ &\quad + \frac{1}{2} \sum_{i=m,s} (U_b + \dot{r}_i + \Omega_b \times r_i)^T m_i (U_b + \dot{r}_i + \Omega_b \times r_i) \end{aligned} \quad (3)$$

where

$$\tilde{M} = \begin{pmatrix} m_b I + M_f & (m_b \hat{r}_b + D_f)^T \\ m_b \hat{r}_b + D_f & J_b + J_f + m_b \hat{r}_b^T \hat{r}_b \end{pmatrix}.$$

In order to distinguish between position vectors and momentum variables, we attach the r_i ($i = b, m, s$) to the position of the i part in the body-fixed frame. The m_i ($i = b, f, m, s$) represent the mass of the i part. J_b is the rotational inertial for the uniformly distributed m_b . Furthermore, it is known that the dots of translational and total angular momentum are external force and external moment, respectively. Hence, according to (1) and (2), the dots take the forms as follows:

$$\begin{aligned} \dot{P} &= P \times \Omega_b + R^T \sum_{i=1}^I f_{\text{ext}_i} \\ \dot{\Pi} &= \Pi \times \Omega_b + P \times U_b + R^T \sum_{j=1}^J \tau_{\text{ext}_j}. \end{aligned} \quad (4)$$

The translational and total angular momentum can be obtained as

$$\begin{aligned} P &= \frac{\partial T}{\partial U_b} = (m_b I + M_f) U_b \\ &\quad + (m_b \hat{r}_b + D_f)^T \Omega_b + \sum_{i=m,s} m_i (U_b + \dot{r}_i + \Omega_b \times r_i) \\ \Pi &= \frac{\partial T}{\partial \Omega_b} = (J_b + J_f + m_b \hat{r}_b^T \hat{r}_b) \Omega_b \\ &\quad + (m_b \hat{r}_b + D_f) U_b + \sum_{i=m,s} m_i \hat{r}_i (U_b + \dot{r}_i + \Omega_b \times r_i). \end{aligned} \quad (5)$$

For convenience of analysis and presentation, some parameters are defined first

$$\begin{aligned} \tilde{M}_b &= \sum_{j=b,m,s} m_j I + M_f \\ D &= \sum_{j=b,m,s} m_j \hat{r}_j + D_f \\ J &= J_b + J_f + \sum_{j=b,m,s} m_j \hat{r}_j^T \hat{r}_j. \end{aligned}$$

Furthermore, substitute (5) and its dot into (4), we can obtain two equations for gliding motion

$$\begin{aligned} \tilde{M}_b \dot{U}_b + D^T \dot{\Omega}_b &= (\tilde{M}_b U_b) \times \Omega_b + (D^T \Omega_b) \times \Omega_b \\ &+ \sum_{i=m,s} m_i (2\dot{r}_i \times \Omega_b - \ddot{r}_i) + R^T \sum_{i=1}^I f_{\text{ext}_i}, \quad (6) \\ D \dot{U}_b + J \dot{\Omega}_b &= (\tilde{M}_b U_b) \times U_b + (D^T \Omega_b) \times U_b \\ &+ (D U_b) \times \Omega_b + (J \Omega_b) \times \Omega_b \\ &+ \sum_{i=m,s} m_i (\hat{r}_i (2\dot{r}_i \Omega_b - \ddot{r}_i)) + R^T \sum_{k=1}^K \tau_{\text{ext}_k}. \quad (7) \end{aligned}$$

As for the dolphin-like motion, we apply the Newton–Euler method for each joint, and their own dynamics can be obtained. Next, by transferring the velocity and forces to body frame, the dynamic model with gliding and dolphin-like motions can be derived based on our previous works [32]

$$M \dot{V}_b = -\Pi_e + \Pi_c + \Pi_h + \Pi_g + \Gamma_m + \Gamma_s \quad (8)$$

where

$$\begin{aligned} M &= \sum_{i=b,w,t,l,r} {}^b H_i M_i {}^i H_b \\ \Pi_c &= - \sum_{i=b,w,t,l,r} {}^b H_i \Gamma_{ci} \\ \Pi_h &= \sum_{i=b,w,t,l,r} {}^b H_i \Gamma_{hi} \\ \Pi_g &= G_b \\ \Gamma_m &= m_m \begin{pmatrix} 2\dot{\hat{r}}_m \Omega_b - \ddot{r}_m \\ \hat{r}_m (2\dot{\hat{r}}_m \Omega_b - \ddot{r}_m) \end{pmatrix} \\ \Gamma_s &= m_s \begin{pmatrix} 2\dot{\hat{r}}_s \Omega_b - \ddot{r}_s \\ \hat{r}_s (2\dot{\hat{r}}_s \Omega_b - \ddot{r}_s) \end{pmatrix} \\ \Pi_e &= \sum_{i=b,w,t,l,r} {}^b H_i M_i (\xi_i + \delta_i) + {}^b H_t M_t {}^t H_w (\xi_w + \delta_w). \end{aligned}$$

IV. DEPTH CONTROL WITH GLIDING MOTION

A. Simplified Plant Model and System Framework

This section presents a depth control system to achieve the target depth in the gliding motion of a robotic dolphin. Taking the calculation efficiency of an embedded platform into consideration, a simplified model is applied for the MPC method. In this article, we just only consider the dynamic model of the vertical plane. Therefore, we assume that the motions of yaw and roll are negligible in this model. Generally, the model neglecting the nonlinear coupling can be obtained as

$$M \dot{v} = -C(v)v - Dv + \tau \quad (9)$$

where $v = [u, w, q]^T$ denotes the forward velocity, diving velocity, and angular velocity about the y-axis w.r.t. body frame, respectively. $M = \text{diag}\{m_1, m_2, m_3\}$ represents the rigid body inertia including added mass. $D = \text{diag}\{d_1, d_2, d_3\}$ is the damping matrix which is simplified to a constant matrix. $\tau = [0, u_c, \tilde{a}G_m \sin(\theta)]$ illustrates the net buoyancy vector, in which u_c denotes the control signal, i.e., net buoyancy, \tilde{a} represents the distance between center of gravity and buoyancy, and

G_m is the gravity of the robot. As for the $C(v)$, it is Coriolis and Centripetal matrix, which can be defined as

$$C(v) = \begin{pmatrix} 0 & 0 & m_2 w \\ 0 & 0 & -m_1 u \\ -m_2 w & m_1 u & 0 \end{pmatrix}.$$

Therefore, the diving velocity dynamic based on (9) can be formalized as

$$\dot{w} = -\frac{d_2}{m_2} w + \frac{u_c}{m_2} - \frac{m_1}{m_2} u q. \quad (10)$$

In particular, the basic principle of the depth control system is adjusting net buoyancy to control diving speed by moving the piston of pipe, further changing the volume of the pipe. As demonstrated in (10), the diving speed is coupled to forward speed u and pitch angular velocity w , so these two variables should be calculated in the whole control process. Nevertheless, it is considerably inconvenience to acquire the gliding states directly, and the capable sensors such as Doppler are improper to our system due to their large sizes and expensive prices. Therefore, a sliding model observer is particularly designed to estimate the gliding states by means of a depth sensor and an IMU. Moreover, since the simple model neglects the motions of yaw and roll, we should guarantee the stability in two motions, which can reduce the effect of model inaccuracy to some extent. On the one hand, due to the bionic shape, an assumption that the gliding robotic dolphin can maintain the stability of the roll direction can be made. On the other hand, the robot may deflect easily in yaw motion owing to the asymmetric hydrodynamic forces generated by both flippers which may be with some mechanical clearance. Therefore, a heading controller based on PID is particularly designed in our control system. Furthermore, the output of MPC is net buoyancy, based on which the position of the pipe piston can be obtained. However, there are many risks of damage when the motor is set in the position mode due to the large acceleration and deceleration. Consequently, in order to protect the buoyancy-driven mechanism motor, we have to choose the speed mode of the motor, and set up the position loop with PID to reduce excessive acceleration and deceleration. The framework of the depth control system is illustrated in Fig. 3.

B. Sliding Mode Observer and Heading Controller Design

According to the dynamic model in (10), we should calculate the predictive diving speed in real time. Hence, u and q should also be attained. However, it may be inaccurate to obtain the velocity vector just by means of the simplified dynamic model. Therefore, an SMO is applied to decrease the estimated error. The diving speed and attitude information can be measured by depth sensor and IMU, respectively. Based on the obtained sensor data, we can estimate the forward speed.

First, the real diving speed w.r.t. inertial frame can be calculated by depth sensor as (11). Denoting ${}^s \dot{U}_{bz}$ as the estimated velocity, the estimation error can be defined as s

$$\begin{aligned} {}^s U_{bz} &= \dot{d} \\ s &= {}^s U_{bz} - {}^s \dot{U}_{bz}. \end{aligned} \quad (11)$$

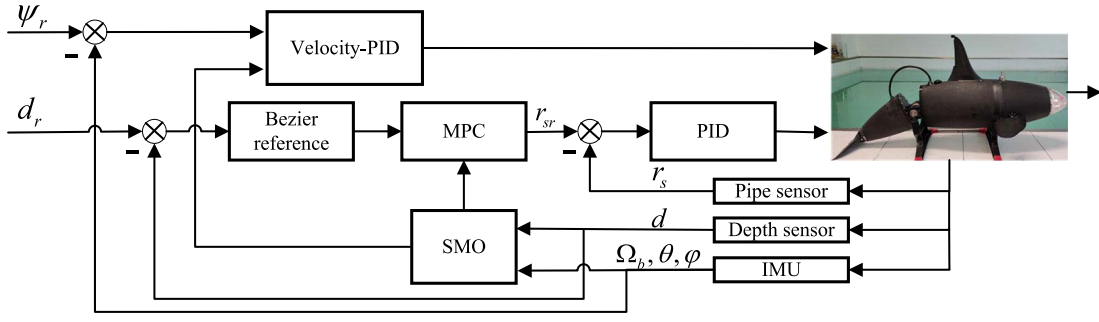


Fig. 3. Framework of depth control system.

Based on the kinematics in (2) and estimation error, the SMO can be designed as follows:

$${}^s\dot{\tilde{U}}_b = {}^sR_b\hat{\Omega}_b\tilde{U}_b + {}^sR_b\dot{\tilde{U}}_b + \begin{pmatrix} c_x \\ c_y \\ c_z \end{pmatrix} \text{sat}(s) \quad (12)$$

where

$$\dot{\tilde{U}}_b = M^{-1}(-C(\tilde{U}_b)\tilde{U}_b - D\tilde{U}_b + \tau).$$

(c_x, c_y, c_z) is the weight vector of SMO. By setting suitable parameters, a Hurwitz matrix can be made to guarantee the convergence of forward speed [12]. Besides, a saturation function $\text{sat}(s)$ is applied to alleviate undesirable chattering effect. Thereafter, the heading controller can be designed based on obtained forward speed.

Regarding the heading control, it should be noted that the control signal refers to the offset angles of flippers. By deflecting the flippers, differential steering moments can be generated, further to produce the steering forces and moments. Due to the relatively poor maneuverability for the gliding motion of the gliding robotic dolphin, the heading control process may be longer and easy to overshoot. Since the steering forces and moments are closely related to speed, we apply a heading controller which exerts larger control signal when the speed of the robot is low, and smaller control signal when the speed is high. This design can decrease the overshoot to some extent. By setting maximum gliding speed of the gliding robotic dolphin v_{\max} , a weight coefficient k_f can be calculated as follows:

$$k_f = \frac{\sqrt{v_x^2 + v_z^2}}{v_{\max}}. \quad (13)$$

Furthermore, based on the yaw error e_ψ , a PID controller is employed to obtain the final control signal as follows:

$$u_f = k_f \left(k_p e_\psi + k_i \int e_\psi + k_d \dot{e}_\psi \right). \quad (14)$$

C. Depth Controller Design

Based on the diving dynamic in (10), we apply the model predictive methodology to design a depth controller. On the one hand, it is owing to the MPC method is suitable to the constrained and large delay system, which is the main characteristic of gliding motion control. On the other hand, the

method has less requirements for model accuracy, which is in line with underwater robot control. The discrete form of diving dynamic can be derived by

$$w(k+1) = Aw(k) + Bu_c(k) + L(k) \quad (15)$$

where

$$\begin{aligned} A &= 1 - \frac{d_2}{m_2} \\ B &= \frac{1}{m_2} \\ L &= -\frac{m_1}{m_2} u(k)q(k). \end{aligned}$$

For better explanation of MPC method, we define the state variable as

$$\xi(k|t) = \begin{pmatrix} w(k|t) \\ u_c(k-1|t) \end{pmatrix}$$

where $(k|t)$ represents the predicted value of the future k time based on the time t . Afterward, the dynamic in (15) can be formalized as

$$\begin{aligned} \xi(k+1|t) &= \tilde{A}\xi(k|t) + \tilde{B}\Delta u_c(k|t) + \tilde{L}(t) \\ \eta(k|t) &= \tilde{C}\xi(k|t) \end{aligned} \quad (16)$$

where

$$\tilde{A} = \begin{pmatrix} A & B \\ 0 & 1 \end{pmatrix}; \tilde{B} = \begin{pmatrix} B \\ 1 \end{pmatrix}; \tilde{C} = (1 \quad 0); \tilde{L} = \begin{pmatrix} L \\ 0 \end{pmatrix}.$$

Moreover, we denote the N_c and N_p as the control and predictive steps, respectively. Hence, the future states can be derived by iteration calculation

$$\begin{aligned} \xi(k+2|t) &= \tilde{A}^2\xi(k|t) + \tilde{A}\tilde{B}\Delta u_c(k|t) + \tilde{B}\Delta u_c(k+1|t) + \tilde{L}(t) \\ &\vdots \\ \xi(k+N_c|t) &= \tilde{A}^{N_c}\xi(k|t) + \tilde{A}^{N_c-1}\tilde{B}\Delta u_c(k|t) + \cdots \\ &\quad + \tilde{B}\Delta u_c(k+N_c-1|t) + \left(\sum_{i=0}^{N_c-1} \tilde{A}^i \right) \tilde{L}(t) \\ &\vdots \\ \xi(k+N_p|t) &= \tilde{A}^{N_p}\xi(k|t) + \tilde{A}^{N_p-1}\tilde{B}\Delta u_c(k|t) + \cdots \\ &\quad + \tilde{A}^{N_p-N_c-1}\tilde{B}\Delta u_c(k+N_c|t) + \left(\sum_{i=0}^{N_p-1} \tilde{A}^i \right) \tilde{L}(t). \end{aligned} \quad (17)$$

Especially, we assume that L item keeps a constant in one predictive process to decouple the diving speed with forward speed and pitch angular. Move one step further, we can obtain the final form by combining (16) with (17)

$$Y(t) = \Upsilon \xi(k|t) + H \Delta U_c(t) + \Delta \quad (18)$$

where

$$\begin{aligned} Y(t) &= (\eta(k+1|t), \dots, \eta(k+N_c|t), \dots, \eta(k+N_p|t))^T \\ \Upsilon &= (\tilde{C}\tilde{A}, \dots, \tilde{C}\tilde{A}^{N_c}, \dots, \tilde{C}\tilde{A}^{N_p})^T \\ \Delta &= \left(I, \dots, \sum_{i=0}^{N_c-1} \tilde{A}, \dots, \sum_{i=0}^{N_p-1} \tilde{A} \right)^T \tilde{L}(t) \\ H &= \begin{pmatrix} \tilde{C}\tilde{B} & 0 & \dots & 0 \\ \vdots & \dots & \ddots & \vdots \\ \tilde{C}\tilde{A}^{N_c-1}\tilde{B} & \dots & \dots & \tilde{C}\tilde{B} \\ \vdots & \dots & \dots & \vdots \\ \tilde{C}\tilde{A}^{N_p-1}\tilde{B} & \dots & \dots & \tilde{C}\tilde{A}^{N_p-N_c-1}\tilde{B} \end{pmatrix}. \end{aligned}$$

Afterward, the optimal solution of control signal is calculated by optimizing an objective function for MPC method. The selection of this function should be considered via two factors. First, the steady error, the difference between the target depth and achieved depth, should be controlled to minimum. In this article, we transform the controlled the target from depth to diving speed. By designing the suitable reference trajectory of diving speed, the target depth can be arrived. Second, the control increment cannot be drastic, otherwise it may cause mechanical and electrical damage of the robot. Based on the above considerations, we adopt the objective function as follows:

$$\begin{aligned} J(\xi(t), \Delta U_c(t)) &= \sum_{i=1}^{N_p} \|\eta(t+i|t) - \eta_{\text{ref}}(t+i|t)\|_Q^2 \\ &\quad + \sum_{i=0}^{N_c-1} \|\Delta u_c(t+i|t)\|_R^2 \quad (19) \end{aligned}$$

where Q and R are weight matrix. The first part guarantees the system's ability to follow the reference trajectory. The second one reflects the requirement for a smooth change in control signal.

By setting $E(t) = \Upsilon \xi(k|t) + \Delta - Y_{\text{ref}}(t)$, and substituting (18) into (19), we can get the initial quadratic form of objective function as follows:

$$J(\xi(t), \Delta U_c(t)) = \Delta U_c(t)^T \Omega \Delta U_c(t) + \Psi \Delta U_c(t) + \Phi \quad (20)$$

where

$$\begin{aligned} \Omega &= H^T \tilde{Q} H + \tilde{R} \\ \Psi &= 2E(t)^T \tilde{Q} H \\ \Phi &= E(t)^T \tilde{Q} E(t) \\ \tilde{Q} &= \text{diag} \{Q, \dots, Q\} \\ &\quad N_x \times N_p \\ \tilde{R} &= \text{diag} \{R, \dots, R\}. \\ &\quad N_u \times N_c \end{aligned}$$

It is obviously that Φ is a constant in one optimization process due to the constant matrix \tilde{Q} . The N_x and N_u represent the dimension of state and control variables, respectively. In this article, the state variable is diving speed, and the control variable is net buoyancy. Therefore, on the basis of the above analysis and derivation, we solve the depth control as an optimization issue. The final optimization function and constraints are as follows:

$$\begin{aligned} \min_{\Delta U_c(t)} J(\xi(t), \Delta U_c(t)) &= \Delta U_c(t)^T \Omega \Delta U_c(t) + \Psi \Delta U_c(t) \\ \text{s.t. } \begin{cases} \Delta U_c(t) \in [\Delta U_{c\min}, \Delta U_{c\max}] \\ U_c(t) \in [U_{c\min}, U_{c\max}]. \end{cases} \quad (21) \end{aligned}$$

By calculating the optimal solution, the optimal control increment sequence can be obtained

$$\Delta U_c^* = (\Delta u_c(t)^* \quad \dots \quad \Delta u_c(t+N_c-1)^*)^T. \quad (22)$$

Move one step further, we can attain the final control signal by selecting the first item of (22)

$$u_c(t) = u_c(t-1) + \Delta u_c(t)^*. \quad (23)$$

Since the robot adjusts the net buoyancy by moving the piston of pipe, we should map the control signal to the actual motor execution via calculating the net buoyancy

$$r_{sr} = \frac{u_c(t)}{\rho g S} \quad (24)$$

where r_{sr} illustrates the reference pipe position in real time; ρ denotes the water density; g elucidates gravity acceleration; and S represents the bottom area of pipe.

More importantly, the reference trajectory of diving speed is another key design in-depth control system. For large time-delay systems, a good reference trajectory can be designed to achieve early action and avoid excessive overshoot. Hence, we design the reference trajectory based on the Bezier curve. As we all know, Bezier curves are commonly used to smooth the path. By setting different control points, the curve shapes are changed. Moreover, Bezier curves are also related to time domain. In our depth system, we hope the depth curve can reduce overshoot as much as possible. Therefore, based on the predictive steps, we apply quadratic Bezier curves to the reference trajectory of depth first. Afterward, the dot of depth reference can be calculated to offer the real-time diving speed reference trajectory. The reference trajectory of depth is designed as follows:

$$P_{\text{ref}}(i) = (1-t(i))^2 d + 2t(i)(1-t(i))^2 d_r + t(i)^2 d_r \quad (25)$$

where

$$t = \frac{1}{N_p} (0 \quad 1 \quad \dots \quad N_p).$$

d_r denotes the target depth, and d represents the real-time depth. Thereafter, the reference trajectory of diving speed can be derived by $V_{\text{ref}} = \dot{P}_{\text{ref}}$. To further control the diving speed better, we employ a segmented reference trajectory. By setting the depth threshold $d_{\text{threshold}}$ and segmented parameters, the final reference trajectory of diving speed can be formalized by

$$Y_{\text{ref}} = \begin{cases} c_1 V_{\text{ref}} & \text{if } |d_r - d| > d_{\text{threshold}} \\ c_2 V_{\text{ref}} & \text{otherwise} \end{cases} \quad (26)$$

Algorithm 1 Algorithm for Control System

```

1: Simplify the dynamic model and discrete it
2: Initialize the model and control parameters
3: repeat
4:   Obtain the depth and attitude data from sensors
5:   Calculate the estimated velocity by SMO of (12)
6:   repeat Heading control module
7:     Use the estimated velocity to get  $k_f$  in (13)
8:     Apply the  $k_f$  to PID controller of (14)
9:   until  $\psi_e < \psi_{threshold}$ 
10:  repeat Depth control module
11:    Optimize the reference tracking by (25) and (26)
12:    Calculate the  $N_p$ -steps model outputs by (18)
13:    Obtain the  $\Omega, \Psi, \Phi, \tilde{Q}, \tilde{R}$  by (20)
14:    Solve the  $N_c$ -steps control outputs of (21) by
        calculating the gradient
15:    Select the first control increment as the final output
16:  until  $d_e < d_{threshold}$ 
17: until Received the end command

```

where c_1 and c_2 are weight parameters. In particular, it should be noted that only two segments are designed in this article. Actually, the numbers of segments can be set in accordance with different target depth. In general, there can be more segments with large target depth, or a continuous function can be applied to illustrate. In order to illustrate the control procedure more clearly, we present the algorithm flowchart as Algorithm 1.

V. SIMULATIONS AND EXPERIMENTS

In this section, the results of extensive simulations and experiments are presented to demonstrate the effectiveness of the proposed depth control system for the gliding robotic dolphin. Simulations were carried out in MATLAB/Simulink under the full-state dynamic model of Section III. The mechanical parameters of simulations tabulated in [32] were measured by Solidworks. Furthermore, the aquatic experiments were conducted in a pool with the dimension of 5-m long, 4-m wide, and 1.05-m deep. Besides, an underwater video camera was applied to record the experimental process, and a secure digital memory (SD) card was employed to record the onboard sensor information for further analysis.

A. Simulation Results and Analysis

Extensive cases of depth control with various parameters were simulated, in which the target depth was set as 0.6 m. There were some parameters that needed to be set manually in our depth system, such as predictive steps N_p , control steps N_c , weight coefficients Q and R , reference tracking coefficients c_1 and c_2 , and so on. Consequently, various simulations were conducted to compare the performances under different parameters, which also provided a valuable reference for the parameters of the following aquatic experiments. First, Q and R make a decisive influence on the results of depth control, in which larger Q leads to smaller steady error, and smaller R means more violent control signal. However, we

TABLE II
MODEL PARAMETERS OF THE DEPTH CONTROL SYSTEM

Parameters	Value	Parameters	Value
m_{11}	11 kg	d_{11}	17 kg/s
m_{22}	13 kg	d_{22}	11 kg/s
m_{33}	0.6 kg·m ²	d_{33}	1.5 kg·m ² /s

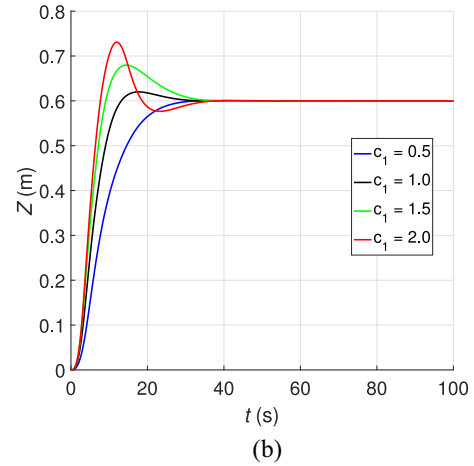
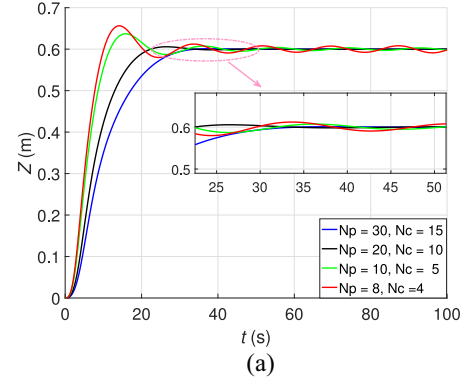


Fig. 4. Simulations of depth control with parameters. (a) Results under different N_p . (b) Results under different c_1 .

have employed a PID controller to make injector work on speed mode, which greatly reduced the failure rate of mechanical damage. Therefore, through the comparison of simulations, we set Q and R as 20 and 0.2, respectively. Second, N_c was set as the half of N_p in the depth system, and c_2 was set as 0.4 in simulations. Regarding the other model parameters, they were tabulated in Table II. Further, we just present the results under different N_p and c_1 in this section, as shown in Fig. 4.

In Fig. 4(a), results under four combinations of N_p and N_c are offered. Especially, smaller N_p may cause the overshoot owing to a lack of ability to predict the future. However, large predictive steps will increase the computational burden. Through evaluating the results from the aspects of both overshoot and response time, it can be seen that the robot performed better when N_p were 20 and 30. In a similar way, by setting different c_1 , we can draw the conclusion that larger c_1 can also lead to overshoot. In essence, larger c_1 means to set higher diving speed to be reference tracking. However, the

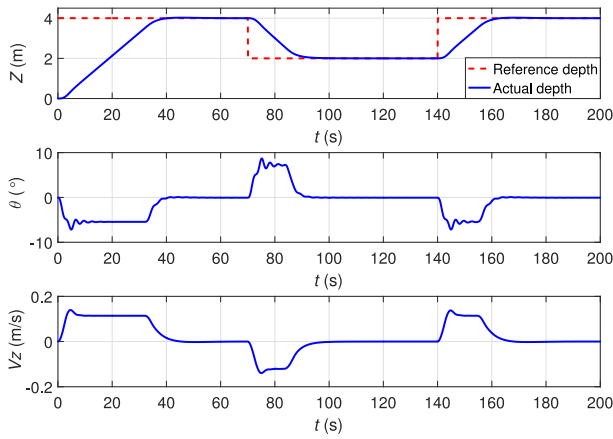


Fig. 5. Results of the depth switching in simulation.

response time with a larger c_1 is not short due to the overshoot. Therefore, the choices of c_1 and c_2 depend on the target depth. When target depth is large enough, the corresponding value of c_1 should be larger. Furthermore, a depth switching simulation was also carried out, in which the target depth was successively set as 2 m, 4 m, and 2 m, as is figured in Fig. 5. It should be noted that N_p , c_1 , and c_2 were set at 30, 1.5, and 0.5 in this simulation, respectively. The result of depth shows no overshoot. Actually, the depth switching experiments are more suitable to large depth due to the large delay characteristics of buoyancy-driven mechanism. As illustrated in the starting stage of depth switching of Fig. 5, the robot performed relatively slow response, and the pitch angle and diving speed reached a stable value after a while. Besides, the maximum diving speed in Fig. 5 is approximately 0.1 m/s, which offers the parameter v_{\max} in heading control.

B. Experimental Results and Analysis Without Slider

We first obtained a relatively optimal parameter set based on a variety of simulations, and applied these parameters to experiments based on minor adjustments. Therefore, the model and control parameters above were employed to test the depth control system in aquatic experiments. The difference lied in that the heading control worked. Moreover, N_p and N_c were set as 30 and 15 in this section, respectively.

1) *Results of Depth Control:* First, the basic experiments of depth control without a movable slider were tested. Via setting the target depth as 0.6 m, the gliding robotic dolphin has successfully realized the depth control, the snapshot of which is figured in Fig. 6. Meanwhile, the depth, pitch angle, and control signal are illustrated in Fig. 7. Especially, we set c_1 as 0.2 due to the small target depth, which signified that the control signal in experiments was small. The advantage of that is the result curve shows very smooth with no overshoot. As for the c_2 and $d_{\text{threshold}}$, they were set as 1.1 and 0.05, respectively. As was demonstrated, the robot arrived the target depth when $t = 30$ s, and the pitch angle achieved the steady state when $t = 20$ s which was earlier than depth. The reason for that may be owing to the large delay system. Besides, the robot had a slight upward trend in about 50 s. There may be two main reasons

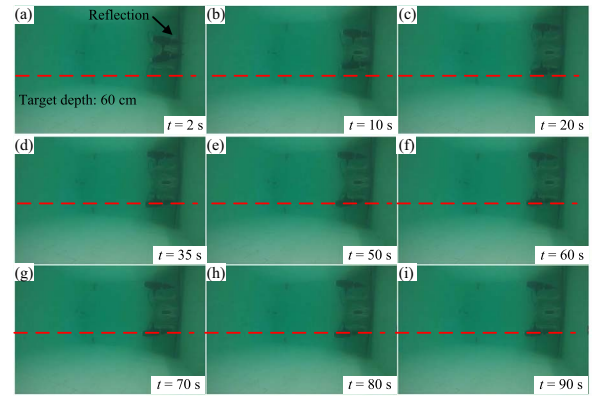


Fig. 6. Snapshot sequences of depth control without a slider.

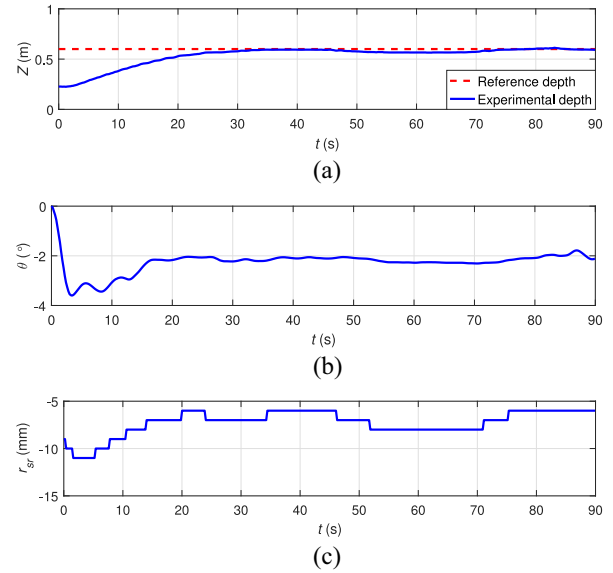


Fig. 7. Experimental results of basic depth control. (a) Depth. (b) Pitch angle. (c) Control signal.

that contribute to the phenomenon. On the one hand, there was a slight water flow disturbance in the underwater environment, which may make the robot shake slightly. On the other hand, some bubbles may be sometimes generated on the robot due to the insufficient smoothness of the robot shell, which could lead to the change of the whole displacement. Certainly, the ability of the robot to resist these effects is also insufficient since the robot has a small overall weight and net mass. When the depth error increased, the robot went back to the target depth with the adjustment of controllers. More importantly, based on the depth results, both the mean absolute error (MAE) and root mean square error (RMSE) were analyzed to discuss the control accuracy and performance of the proposed control method. When the gliding robotic dolphin entered the steady state at $t = 30$ s, the RMSE and MAE of control error were 2.1 cm and 1.67 cm, respectively, which demonstrated the effectiveness of depth control. Note that we manually set a bias for the control signal to ensure that the robot remained hovering when there was no control, that was, the total displacement was equal to the total weight of

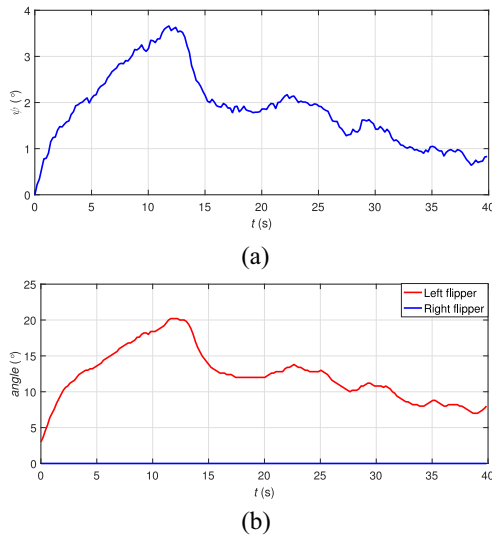


Fig. 8. Heading control results of basic depth control. (a) Yaw angle. (b) Flippers' angle.

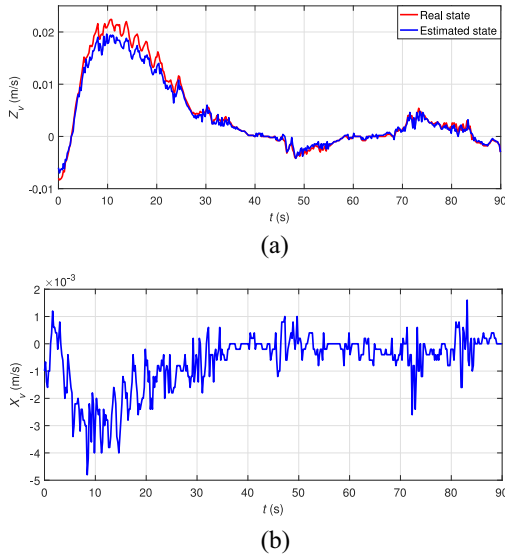


Fig. 9. SMO results of basic depth control. (a) Diving speed Z_v . (b) Forward speed X_v .

the robot. This bias can be used to balance the small volume changes due to external disturbances, such as bubbles.

2) *Results of Heading Control and SMO*: Moreover, the performances of heading control and SMO were also investigated, the results of which are shown in Figs. 8 and 9. In experiments, we set the initial yaw angle as the target, which meant that the objective was to keep the heading of the robot unchanged. In essence, the basic principle of the regulation method is to use differential actions of the flippers to generate asymmetric hydrodynamic forces. For instance, when the robot deviates to the left direction, the left flipper will deflect while the right flipper keeps still. In an aspect of the heading control process of Fig. 8, we can see the robot tended to departure from the target when the speed started to increase. Afterward, the flippers started to deflect, and the flippers' angles were calculated by (14) which was related with speed.

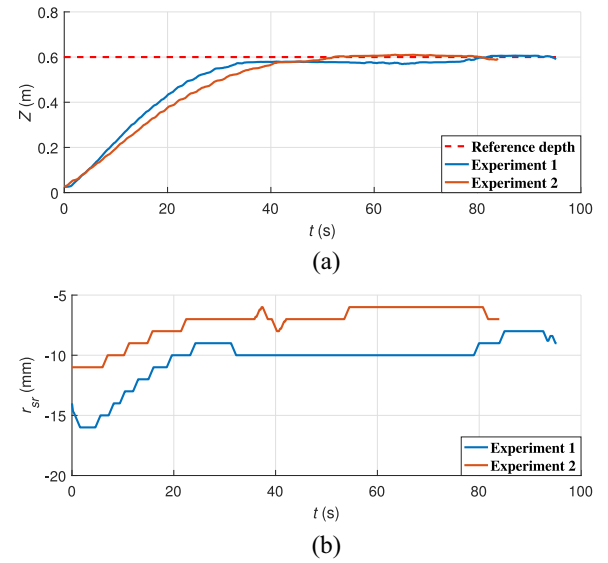


Fig. 10. Experimental results of extended depth control. (a) Depth. (b) Control signal.

Consequently, the yaw angle gradually returned to the target yaw. More importantly, it should be noted that the heading control was only executed during a part of the control process. When the distance from the target depth was less than a certain threshold, heading control would be suspended. The reason for this design is that the robot almost has no speed in the final stage of depth control, so the heading control with the deflecting method is unnecessary to exert. Regarding the SMO results plotted in Fig. 9, the estimated diving speed is approximately consistent with the real. Meanwhile, the forward speed is estimated to be near zero, which can be seen that the robot almost dived just along the vertical plane in snapshot sequences. As a matter of fact, the heading control and SMO are applied to assist in-depth control. Therefore, the accuracy is within the acceptable range. Further, through decreasing the model error between the simplified model and actual plant model, the accuracy of SMO can be improved.

3) *Results of Extended Experiments*: In order to further validate the effectiveness of the proposed method, we conducted more extended aquatic experiments. Fig. 10 illustrates the depth control with better performance than that in the basic experiment. In the first experiment, the RMSE and MAE of depth error were 2.0 cm and 1.82 cm, respectively. Moreover, the RMSE and MAE of depth error in the second experiment were 0.68 cm and 0.63 cm, respectively, which performed much better in both two criteria. Compared with the first experiment, the control signal of the second experiment was a little smaller in the whole control process, which directly led to longer response time. In addition, another reason for the difference of control signal in two experiments was the difference of control bias mentioned in the above discussion. Furthermore, another aquatic experiment focused on depth control under different target depth. Considering the limitation of pool size, the experiments under target depth which ranged from 0.3 m to 0.5 m were carried out, as is plotted in Fig. 11. When the robot entered the steady state, we calculated the RMSE

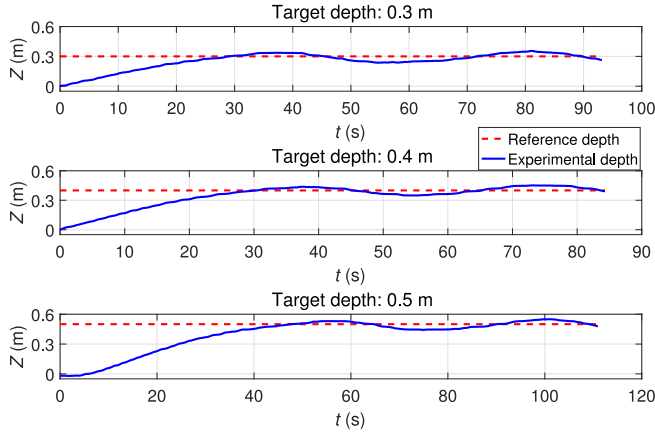
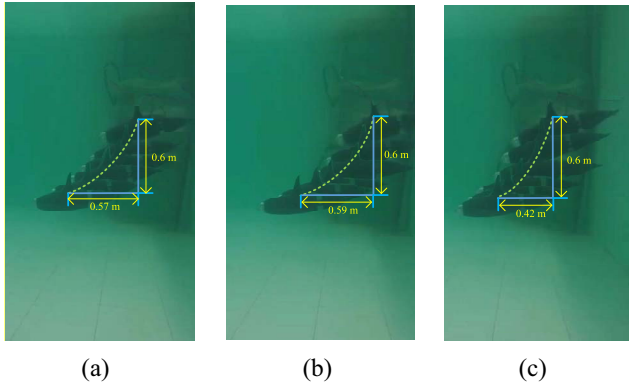


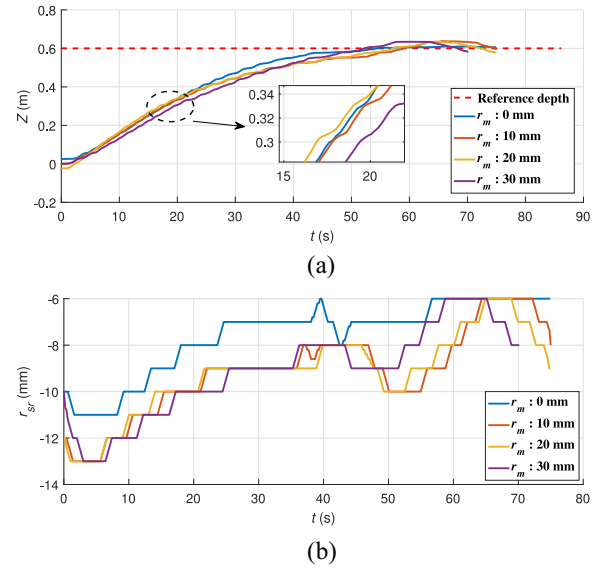
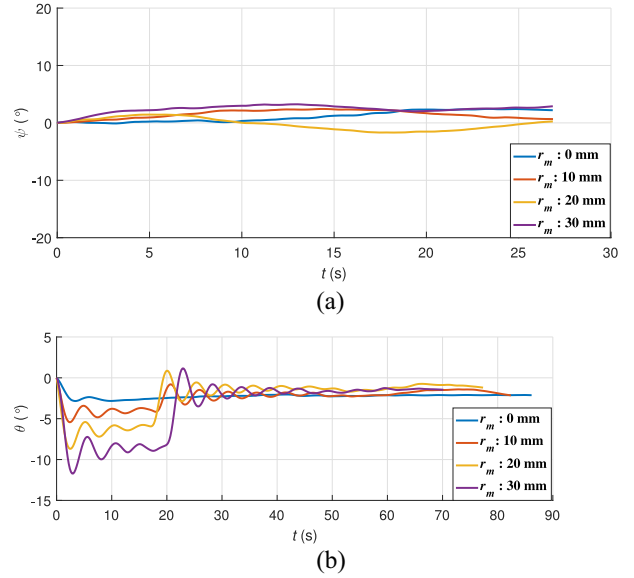
Fig. 11. Depth results under different target depth.

Fig. 12. Snapshot sequences of experiments under different slider positions. (a) $r_m = 10$ mm. (b) $r_m = 20$ mm. (c) $r_m = 30$ mm.

and MAE of steady-state error. The RMSEs of the 30–50 cm control target were approximately 3.56 cm, 3.3 cm, and 3.35 cm, respectively, while their MAEs were approximately 3.13 cm, 2.86 cm, and 2.87 cm, respectively. More careful inspection shows that the error has slight undulation. There may be two reasons for this phenomenon, e.g., small target depth and unsuitable parameters of the controller. Since the delay characteristics, the response of the robot is not sensitive. Especially, when the target depth is small, the robot is easier to perform overshooting. As a result, it is more suitable for the gliding robotic dolphin to realize depth control under large target depth.

C. Experimental Results With Slider

Moreover, we also investigated the effect of a movable slider during the depth control process. In experiments, we set the position of the slider from 10 mm to 30 mm, and the heading control was also employed. In particular, it should be noted that we moved the slider to the target position at the initial stage, and moved back to zero when the robot arrived the 0.3-m depth, which contributed to the steady depth control in the final stage. In Fig. 12, the snapshot sequences of depth control experiments under three slider positions are illustrated, and the lateral and longitudinal distances of the gliding are marked out, which shows the orders of the lateral distance

Fig. 13. Experimental results of depth control under different r_m . (a) Depth. (b) Control signal.Fig. 14. Angle results of depth control under different r_m . (a) Yaw angle. (b) Pitch angle.

is $x_{20\text{ mm}} > x_{10\text{ mm}} > x_{30\text{ mm}}$. Figs. 13 and 14 reveal the depth and angle under different slider positions, respectively. Besides, the results of depth and yaw angle validate the robot can successfully realize the depth and heading control with a slider. Especially, in the initial stage of Fig. 13, the diving speed with $r_m = 30$ mm was the smallest, the reason for which may be that the attitude of the body was not adjusted to stable state in time. This point can also be verified by pitch angle in Fig. 14. Therefore, the robot with $r_m = 30$ mm was late to reach a depth of 0.3 m. In addition, it can be found that the robot with $r_m = 20$ mm was the first one to achieve the 0.3-m depth at $t = 17$ s. Hence, its pitch angle came back much earlier, which contributed to its large horizontal distance due to a small gliding angle. Moreover, the moving of the injector piston may also make some influence on the attitude

and depth results since it can also change the center of gravity. For instance, the robot with $r_m = 30$ mm kept relatively long time in the state of large r_{sr} , which signified the injector piston had more effect on the gravity's center shift. Therefore, we can draw the conclusion to some extent that the robot can achieve different gliding angles by moving the slider during the depth control process, which can be used to further control the horizontal gliding distance.

D. Discussion

Due to the large delay and poor maneuverability of buoyancy-driven underwater robot, it is hard to achieve motion control with high precision. The gliding robotic dolphin, as a hybrid underwater robot, is particularly designed to overcome the weaknesses through combining the robotic dolphin and underwater gliders. Therefore, in order to explore the performance of the gliding robotic dolphin in the vertical plane, high precision depth control only by an injector-based buoyancy mechanism has been successfully realized in this article. Meanwhile, the effects of movable sliders for gliding angle in-depth control process are also investigated, which not only validates the feasibility of the platform and proposed control framework but also accumulates valuable engineering experience for the ocean exploration. Compared with depth control of traditional underwater robots [17], the gliding robotic dolphin has more excellent maneuverability due to the rotatable surfaces, for example, the heading control is achieved via deflecting the flippers. Compared with the results in [23], although the size of our robot is much larger than them, we still achieve the better performance in aspect of depth error. Additionally, an MPC controller, a heading controller, and an SMO are programmed by C language, and applied to an embedded platform with float point unit (FPU). In order to reduce the computing burden, the dynamic model is simplified. Hence, the real-time performance is improved to some extent.

In spite of successful depth control exerted on the gliding robotic dolphin, there are some limitations on some aspects. First, since the injector changes buoyancy by sucking and draining, it needs to overcome water pressure when draining, which means it is much difficult to accomplish the buoyancy adjustment in the deep water environment. To address this issue, high power motor or internal liquid bladders can be applied, yet the latter design need enough internal space. Second, due to the simplified model error and inaccurate parameters, the estimation accuracy of SMO is not particularly high. Through enhancing the model accuracy or taking other estimation method, such as the Kalman filter, the problem can be improved. Third, regarding the real-time computing, the calculated control signal seems a little unsmooth. By carrying a more efficient master chip or appropriately decreasing predictive steps, the MPC can run faster. The improvements for state estimation and faster computing are ongoing endeavors.

VI. CONCLUSION

In this article, we have developed a novel depth control system with a movable slider to a gliding robotic dolphin.

Considering the motion characteristics, we propose a novel control strategy consisting of an MPC controller, a heading controller, and an SMO for precise depth control of a gliding robotic dolphin. First, a simplified model is used to reduce computing burden in the MPC controller, in which the reference tracking is improved by the Bezier curve. Second, a velocity-based PID controller is designed to control the heading direction on the basis of ignoring the slight yaw motion. In order to estimate the velocity, an SMO is constructed based on the information of the IMU and depth sensor. Finally, extensive simulations and aquatic experiments have demonstrated the effectiveness of the proposed control system. Moreover, some aquatic experiments are also conducted to explore how the movable slider affects the gliding angle in depth control, not in-depth control. It is revealed that the movable slider can be applied to obtain regular gliding angles during the depth control process, which offers a promising prospect to realize trajectory tracking in the vertical plane. Remarkably, the obtained results and analysis provide valuable insight into the accomplishment of complex ocean tasks for the gliding robotic dolphin.

In the future, we plan to further improve the system performance, especially, the state estimation and computing efficiency. In the meantime, we will explore the specific relationship between the slider position and gliding angle based on the investigation of the 3-D path following via hybrid motions.

REFERENCES

- [1] R. K. Katzschmann, J. DelPreto, R. MacCurdy, and D. Rus, "Exploration of underwater life with an acoustically controlled soft robotic fish," *Sci. Robot.*, vol. 3, no. 16, 2018, Art. no. eaar3449.
- [2] R. Wang, S. Wang, Y. Wang, M. Tan, and J. Yu, "A paradigm for path following control of a ribbon-fin propelled biomimetic underwater vehicle," *IEEE Trans. Syst., Man, Cybern., Syst.*, vol. 49, no. 3, pp. 482–493, Mar. 2019.
- [3] K. Alam, T. Ray, and S. G. Anavatti, "Design optimization of an unmanned underwater vehicle using low- and high-fidelity models," *IEEE Trans. Syst., Man, Cybern., Syst.*, vol. 47, no. 11, pp. 2794–2808, Nov. 2017.
- [4] J. Yu, Z. Su, M. Wang, M. Tan, and J. Zhang, "Control of yaw and pitch maneuvers of a multilink dolphin robot," *IEEE Trans. Robot.*, vol. 28, no. 2, pp. 318–329, Apr. 2012.
- [5] J. Yu, Z. Su, Z. Wu, and M. Tan, "An integrative control method for bio-inspired dolphin leaping: Design and experiments," *IEEE Trans. Ind. Electron.*, vol. 63, no. 5, pp. 3108–3116, May 2016.
- [6] J. Yu, Z. Wu, Z. Su, T. Wang, and S. Qi, "Motion control strategies for a repetitive leaping robotic dolphin," *IEEE/ASME Trans. Mechatronics*, vol. 24, no. 3, pp. 913–923, Jun. 2019.
- [7] Z. Wu, J. Liu, J. Yu, and H. Fang, "Development of a novel robotic dolphin and its application to water quality monitoring," *IEEE/ASME Trans. Mechatronics*, vol. 22, no. 5, pp. 2130–2140, Oct. 2017.
- [8] Z. Wu, J. Yu, J. Yuan, and M. Tan, "Towards a gliding robotic dolphin: Design, modeling, and experiments," *IEEE/ASME Trans. Mechatronics*, vol. 24, no. 1, pp. 260–270, Feb. 2019.
- [9] Z. Wu, J. Yu, J. Yuan, M. Tan, and J. Zhang, "Mechatronic design and implementation of a novel gliding robotic dolphin," in *Proc. IEEE Int. Conf. Robot. Biomimetics*, Zhuhai, China, Dec. 2015, pp. 267–272.
- [10] F. Zhang, J. Thon, C. Thon, and X. Tan, "Miniature underwater glider: Design and experimental results," *IEEE/ASME Trans. Mechatronics*, vol. 19, no. 1, pp. 394–399, Feb. 2014.
- [11] J. Sherman, R. E. Davis, W. B. Owens, and J. Valdes, "The autonomous underwater glider 'Spray,'" *IEEE J. Ocean. Eng.*, vol. 26, no. 4, pp. 437–446, Oct. 2001.
- [12] J. Yuan, Z. Wu, J. Yu, and M. Tan, "Sliding mode observer-based heading control for a gliding robotic dolphin," *IEEE Trans. Ind. Electron.*, vol. 64, no. 8, pp. 6815–6824, Aug. 2017.

- [13] Z. Wu, J. Yu, J. Yuan, M. Tan, and S. Qi, "Gliding motion regulation of a robotic dolphin based on a controllable fluke," *IEEE Trans. Ind. Electron.*, to be published, doi: [10.1109/TIE.2019.2913810](https://doi.org/10.1109/TIE.2019.2913810).
- [14] F. Zhang, O. Ennasr, E. Litchman, and X. Tan, "Autonomous sampling of water columns using gliding robotic fish: Algorithms and harmful-algae-sampling experiments," *IEEE Syst. J.*, vol. 10, no. 3, pp. 1271–1281, Sep. 2016.
- [15] J.-H. Li and P.-M. Lee, "Design of an adaptive nonlinear controller for depth control of an autonomous underwater vehicle," *Ocean Eng.*, vol. 32, nos. 17–18, pp. 2165–2181, 2005.
- [16] C. Silvestre and A. Pascoal, "Depth control of the INFANTE AUV using gain-scheduled reduced order output feedback," *Control Eng. Pract.*, vol. 15, no. 7, pp. 883–895, 2007.
- [17] H. Wu, S. Song, K. You, and C. Wu, "Depth control of model-free AUVs via reinforcement learning," *IEEE Trans. Syst., Man, Cybern., Syst.*, vol. 49, no. 12, pp. 2499–2510, Dec. 2019, doi: [10.1109/TSMC.2017.2785794](https://doi.org/10.1109/TSMC.2017.2785794).
- [18] N. A. A. Hussain, M. R. Arshad, and R. Mohd-Mokhtar, "Underwater glider modelling and analysis for net buoyancy, depth and pitch angle control," *Ocean Eng.*, vol. 38, no. 16, pp. 1782–1791, 2011.
- [19] M. G. Joo and Z. Qu, "An autonomous underwater vehicle as an underwater glider and its depth control," *Int. J. Control Autom. Syst.*, vol. 13, no. 5, pp. 1212–1220, 2015.
- [20] J. Yu, F. Sun, D. Xu, and M. Tan, "Embedded vision-guided 3-D tracking control for robotic fish," *IEEE Trans. Ind. Electron.*, vol. 63, no. 1, pp. 355–363, Jan. 2016.
- [21] J. Yu, J. Liu, Z. Wu, and H. Fang, "Depth control of a bioinspired robotic dolphin based on sliding-mode fuzzy control method," *IEEE Trans. Ind. Electron.*, vol. 65, no. 3, pp. 2429–2438, Mar. 2018.
- [22] F. Shen, Z. Cao, C. Zhou, D. Xu, and N. Gu, "Depth control for robotic dolphin based on fuzzy PID control," *Int. J. Offshore Polar Eng.*, vol. 23, no. 3, pp. 166–171, 2013.
- [23] M. Makrodimitris, I. Aliprantis, and E. Papadopoulos, "Design and implementation of a low cost, pump-based, depth control of a small robotic fish," in *Proc. IEEE/RSJ Int. Conf. Intell. Robots Syst.*, Chicago, IL, USA, Sep. 2014, pp. 1127–1132.
- [24] Z. Li, J. Deng, R. Lu, Y. Xu, J. Bai, and C.-Y. Su, "Trajectory-tracking control of mobile robot systems incorporating neural-dynamic optimized model predictive approach," *IEEE Trans. Syst., Man, Cybern., Syst.*, vol. 46, no. 6, pp. 740–749, Jun. 2016.
- [25] F. Ke, Z. Li, H. Xiao, and X. Zhang, "Visual servoing of constrained mobile robots based on model predictive control," *IEEE Trans. Syst., Man, Cybern., Syst.*, vol. 47, no. 7, pp. 1428–1438, Jul. 2017.
- [26] M. Yue, C. An, and Z. Li, "Constrained adaptive robust trajectory tracking for WIP vehicles using model predictive control and extended state observer," *IEEE Trans. Syst., Man, Cybern., Syst.*, vol. 48, no. 5, pp. 733–742, May 2018.
- [27] I. Abraham and J. Yi, "Model predictive control of buoyancy propelled autonomous underwater glider," in *Proc. Amer. Control Conf.*, Chicago, IL, USA, Jul. 2015, pp. 1181–1186.
- [28] C. Shen, Y. Shi, and B. Buckham, "Path-following control of an AUV using multi-objective model predictive control," in *Proc. Amer. Control Conf.*, Boston, MA, USA, Jul. 2016, pp. 4507–4512.
- [29] C. Shen, Y. Shi, and B. Buckham, "Nonlinear model predictive control for trajectory tracking of an AUV: A distributed implementation," in *Proc. IEEE Conf. Decis. Control*, Las Vegas, NV, USA, Dec. 2016, pp. 5998–6003.
- [30] D. C. Fernández and G. A. Hollinger, "Model predictive control for underwater robots in ocean waves," *IEEE Robot. Autom. Lett.*, vol. 2, no. 1, pp. 88–95, Jan. 2017.
- [31] J. G. Graver, "Underwater gliders: Dynamics, control, and design," Ph.D. dissertation, Dept. Mech. Aerosp. Eng., Princeton Univ., Princeton, NJ, USA, 2005.
- [32] J. Wang, Z. Wu, Y. Yang, M. Tan, and J. Yu, "Spiraling motion of a gliding robotic dolphin based on the 3-D dynamic model," in *Proc. IEEE Int. Conf. Real Time Comput. Robot.*, Aug. 2018, pp. 13–18.



Jian Wang received the B.E. degree in automation from the University of Science and Technology Beijing, Beijing, China, in 2016. He is currently pursuing the Ph.D. degree in control theory and control engineering with the Institute of Automation, Chinese Academy of Sciences, Beijing.

His research interests include bio-inspired underwater robots and intelligent control systems.



Zhengxing Wu received the B.E. degree in logistics engineering from the School of Control Science and Engineering, Shandong University, Jinan, China, in 2008, and the Ph.D. degree in control theory and control engineering from the Institute of Automation, Chinese Academy of Sciences (IACAS), Beijing, China, in 2015.

He is currently an Associate Professor with the State Key Laboratory of Management and Control for Complex Systems, IACAS. His current research interests include fast maneuvers of bio-inspired robotic fish and gliding motions of robotic dolphins.



Min Tan received the B.Sc. degree in control science and engineering from Tsinghua University, Beijing, China, in 1986, and the Ph.D. degree in control science and engineering from the Institute of Automation, Chinese Academy of Sciences (IACAS), Beijing, China, in 1990.

He is currently a Professor with the State Key Laboratory of Management and Control for Complex Systems, IACAS. He has published more than 200 papers in journals, books, and conference proceedings. His research interests include robotics and intelligent control systems.



Junzhi Yu (SM'14) received the B.E. degree in safety engineering and the M.E. degree in precision instruments and mechatronics from the North University of China, Taiyuan, China, in 1998 and 2001, respectively, and the Ph.D. degree in control theory and control engineering from the Institute of Automation, Chinese Academy of Sciences, Beijing, China, in 2003.

From 2004 to 2006, he was a Post-Doctoral Research Fellow with the Center for Systems and Control, Peking University, Beijing. He was an

Associate Professor with the Institute of Automation, Chinese Academy of Sciences in 2006, where he was a Full Professor in 2012. In 2018, he joined the College of Engineering, Peking University as a Tenured Full Professor. His current research interests include intelligent robots, motion control, and intelligent mechatronic systems.